

# A comparison of different order hybrid finite difference-volume methods for solving the Serre equations in conservative law form

Jordan Pitt,<sup>1</sup>  
Christopher Zoppou,<sup>1</sup>  
Stephen G. Roberts,<sup>1</sup>

## ABSTRACT

In this paper a first-, second- and third-order version of a numerical method for the Serre equations are described. Such a method is described as a finite difference-volume method due to the use of a finite difference approximation and a finite volume method to solve the Serre equations in conservation law form. These methods are then validated and used to investigate a discrepancy in the literature about the results of solving the Serre equations in the presence of steep gradients.

**Keywords:** dispersive waves, conservation laws, Serre equation, finite volume method, finite difference method

## <sup>1</sup> INTRODUCTION

Free surface flows occur in many important applications such as; tsunamis, storm surges and tidal bores. Because viscosity has a negligible effect on these problems the Euler equations can be used to model them. However, numerical methods for the Euler equations are not yet computationally efficient enough to deal with these problems over large domains. Thus various approximations to the Euler equations have been derived, the most crude of which are the shallow water wave equations which have been used to model the named applications in the past. However, the shallow water wave equations assume a hydrostatic pressure distribution in a fluid column which is not fully justified in rapidly varying flows because vertical acceleration inside the fluid becomes important.

---

<sup>1</sup>Mathematical Sciences Institute, Australian National University, Canberra, ACT 0200, Australia, E-mail: Jordan.Pitt@anu.edu.au. The work undertaken by the first author was supported financially by an Australian National University Scholarship.

11 Consequently, many equations have been derived as approximations to the Euler equa-  
12 tions in shallow fluids that are less restrictive in their assumptions than the shallow water  
13 wave equations. The Serre equations are one set of these and do not enforce a hydrostatic  
14 pressure distribution over a fluid column allowing for fully non-linear flows (Lannes and  
15 Bonneton 2009).

16 The Serre equations were first derived by Serre (1953) for flat bottom topographies  
17 in one dimension. Su and Gardner (1969) obtained equations for any smooth bottom  
18 topographies in one dimension and Green and Naghdi (1976) did the same in two dimen-  
19 sions. These equations have been handled in many different ways (Mitsotakis et al. 2014;  
20 Bonneton et al. 2011; Antunes do Carmo et al. 1993; Chazel et al. 2011; Cienfuegos and  
21 Bonneton 2006; Cienfuegos and Bonneton 2007; Dutykh et al. 2011). This paper fol-  
22 lows the decomposition of the Serre equations into conservative law form (Le Métayer  
23 et al. 2010; Li et al. 2014) and then follows the formulation of Le Métayer et al. (2010)  
24 and Zoppou (2014) to build first-, second- and third-order methods. The benefits of this  
25 method are its steep gradient handling capability which this paper will investigate.

26 Zoppou and Roberts (1996) demonstrated that first- and third-order methods produce  
27 diffusive errors smearing steep gradients. While second-order methods produce dissipative  
28 errors introducing non-physical oscillations around steep gradients. Because steep gradi-  
29 ents arise naturally in fluid flows and the Serre equations produce dispersive waves around  
30 them (El et al. 2006) it is important that for the described methods these oscillations are  
31 not significantly polluted by either diffusion or dissipation.

32 This paper aims to clear up the discrepancy between the results of Le Métayer et al.  
33 (2010) and El et al. (2006) by examining the behaviour of a certain dam-break problem.  
34 In particular in Le Métayer et al. (2010) it is stated that their first-order method was suf-  
35 ficient to capture the important behaviour of the dam-break problem, this paper will test  
36 the validity of that assertion. To accomplish this first-, second- and third-order methods  
37 to solve the Serre equations are constructed and validated by comparing the solutions to  
38 known analytical solutions and laboratory data of flows containing steep gradients. Then  
39 the results for a dam-break problem for all described methods are compared to resolve this  
40 conflict.

## 41 **SERRE EQUATIONS**

42 The Serre equations can derived as an approximation to the full Euler equations by  
43 depth integration similar to Su and Gardner (1969). They can also be seen as an asymp-  
44 totic expansion of the Euler equations (Lannes and Bonneton 2009). The former is more  
45 consistent with the perspective from which numerical methods will be developed in this  
46 paper while the latter indicates the appropriate regions in which to use these equations as  
47 a model of fluid flow.

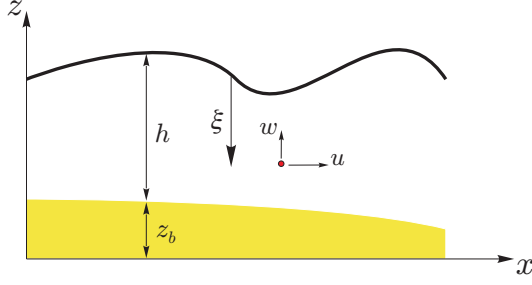


FIG. 1: The notation used for one-dimensional flow governed by the Serre equation.

The scenario under which the Serre approximation is made consists of a two dimensional  $\mathbf{x} = (x, z)$  fluid over a bottom topography as in Figure 1, under the action of gravity. The water depth is  $h(x, t)$  and  $z_b(x)$  is the bed elevation. The fluid is subject to the pressure,  $p(\mathbf{x}, t)$  and gravitational acceleration,  $\mathbf{g} = (0, g)^T$  and has a velocity  $\mathbf{v} = (u(\mathbf{x}, t), w(\mathbf{x}, t))$ , where  $u(\mathbf{x}, t)$  is the velocity in the  $x$ -coordinate and  $w(\mathbf{x}, t)$  is the velocity in the  $z$ -coordinate and  $t$  is time. Assuming that  $z_b(x)$  is constant the Serre equations read (Li et al. 2014; Zoppou 2014)

$$\frac{\partial h}{\partial t} + \frac{\partial(\bar{u}h)}{\partial x} = 0, \quad (1a)$$

$$\underbrace{\frac{\partial(\bar{u}h)}{\partial t} + \frac{\partial}{\partial x} \left( \bar{u}^2 h + \frac{gh^2}{2} \right)}_{\text{Shallow Water Wave Equations}} + \underbrace{\frac{\partial}{\partial x} \left( \frac{h^3}{3} \left[ \frac{\partial \bar{u}}{\partial x} \frac{\partial \bar{u}}{\partial x} - \bar{u} \frac{\partial^2 \bar{u}}{\partial x^2} - \frac{\partial^2 \bar{u}}{\partial x \partial t} \right] \right)}_{\text{Dispersion Terms}} = 0 \quad (1b)$$

Serre Equations

60 where  $\bar{u}$  is the average of  $u$  over the depth of water.

## 61 Alternative Conservation Law Form of the Serre Equations

In Le Métayer et al. (2010) and Zoppou (2014) it is demonstrated that the Serre equations can be rearranged into a conservation law form, by introducing a new quantity

$$G = uh - h^2 \frac{\partial h}{\partial x} \frac{\partial u}{\partial x} - \frac{h^3}{3} \frac{\partial^2 u}{\partial x^2}. \quad (2)$$

66 Consequently, the equations can be rewritten as

$$\frac{\partial h}{\partial t} + \frac{\partial(uh)}{\partial x} = 0 \quad (3a)$$

69 and

70      
$$\frac{\partial G}{\partial t} + \frac{\partial}{\partial x} \left( Gu + \frac{gh^2}{2} - \frac{2h^3}{3} \frac{\partial u}{\partial x} \frac{\partial u}{\partial x} \right) = 0 \quad (3b)$$
  
71

72 where the bar over  $u$  has been dropped to simplify the notation. A hybrid method can  
73 be developed for the Serre equations that solves the elliptic problem (2) for  $u$  and then  
74 the conservation law (3) for  $h$  and  $G$  at some later time. This replicates the process of  
75 Le Métayer et al. (2010) and Zoppou (2014).

76 **NUMERICALLY SOLVING THE SERRE EQUATIONS WRITTEN IN  
77 CONSERVATION LAW FORM**

78 There are numerous ways a numerical method could be built to solve the Serre equa-  
79 tions in conservation law form (3). For flows that contain steep gradients the finite volume  
80 method seems the most appropriate. A finite volume method to solve (3) updates the con-  
81 served quantities  $h$  and  $G$  over a single time step  $\Delta t$  for instance from time  $t^n$  to  $t^{n+1}$ . So  
82 that

83      
$$\begin{bmatrix} h^{n+1} \\ G^{n+1} \end{bmatrix} = \mathcal{L}(h^n, G^n, u^n, \Delta t) \quad (4)$$
  
84

85 where  $\mathcal{L}$  is some numerical solver for (3) and the superscript denotes the time at which a  
86 quantity is evaluated; e.g.  $u^n = u(t^n)$ . The complete solution also involves solving (2) for  
87  $u$  given  $h$  and  $G$  denoted by

88      
$$u^{n+1} = \mathcal{A}(h^{n+1}, G^{n+1}). \quad (5)$$

90

91 **SOLVING THE ELLIPTIC EQUATION  $\mathcal{A}$  FOR  $U$**

92 Assuming that a discretisation in space has a fixed resolution so that  $\forall i x_{i+1} - x_i = \Delta x$ ;  
93 allows for a simple finite difference approximation to (2) as a suitable method for  $\mathcal{A}$   
94 (Le Métayer et al. 2010; Zoppou 2014). Since the goal of this paper is to develop and com-  
95 pare a range of different order methods for this problem both a second- and fourth-order  
96 centred finite difference approximation to (2) were used. By taking such approximations  
97 to the first- and second-order spatial derivatives the second- and fourth-order analogues of  
98 (2) are given by

99      
$$G_i = u_i h_i - h_i^2 \left( \frac{h_{i+1} - h_{i-1}}{2\Delta x} \right) \left( \frac{u_{i+1} - u_{i-1}}{2\Delta x} \right) - \frac{h_i^3}{3} \left( \frac{u_{i+1} - 2u_i + u_{i-1}}{\Delta x^2} \right)$$
  
100

101 and

$$102 \quad G_i = u_i h_i - h_i^2 \left( \frac{-h_{i+2} + 8h_{i+1} - 8h_{i-1} + h_{i-2}}{12\Delta x} \right) \left( \frac{-u_{i+2} + 8u_{i+1} - 8u_{i-1} + u_{i-2}}{12\Delta x} \right)$$

$$103 \quad - \frac{h_i^3}{3} \left( \frac{-u_{i+2} + 16u_{i+1} - 30u_i + 16u_{i-1} - u_{i-2}}{12\Delta x^2} \right)$$

104 where the subscript denotes the spatial coordinate at which the quantity is evaluated; e.g.  
105  $u_i = u(x_i)$ . Both of these can be rearranged into a matrix equation with the following form

$$106 \quad \begin{bmatrix} u_0 \\ \vdots \\ u_m \end{bmatrix} = A^{-1} \begin{bmatrix} G_0 \\ \vdots \\ G_m \end{bmatrix} =: \mathcal{A}(\mathbf{h}, \mathbf{G})$$

$$107$$

108 where for a second-order approximation the matrix  $A$  is tri-diagonal while for a fourth-  
109 order method it is penta-diagonal.

## 110 SOLVING THE CONSERVATION LAW FORM OF THE SERRE EQUATIONS

111 A finite volume method of sufficient order was developed to solve (3). Unlike finite  
112 difference methods which utilise nodal values of quantities, finite volume methods use the  
113 cell averages, for example the average water depth over a cell which spans  $[x_{i-1/2}, x_{i+1/2}]$   
114 is

$$115 \quad \bar{h}_i = \frac{1}{\Delta x} \int_{x_{i-1/2}}^{x_{i+1/2}} h(x, t) dx$$

$$116$$

117 where  $x_{i\pm 1/2} = x_i \pm \Delta x/2$ . Finite volume methods update the cell averages by the following  
118 method

$$119 \quad \bar{U}_i^{n+1} = \bar{U}_i^n - \frac{\Delta t}{\Delta x} \left( F_{i+1/2}^n - F_{i-1/2}^n \right) \quad (6)$$

$$120$$

121 where  $\bar{U}_i^n = [\bar{h}_i^n \bar{G}_i^n]^T$  is an approximation of the vector of the conserved quantities aver-  
122 aged over the cell at time  $t^n$ . While  $F_{i\pm 1/2}^n$  is an approximation of the average flux at the  
123 respective cell boundary  $x_{i\pm 1/2}$  over the time interval  $[t^n, t^{n+1}]$ , which is obtained by solving  
124 the Riemann problem at the cell boundaries.

### 125 Local Riemann Problem

126 Since  $\bar{U}_i^n$  is known what remains is to calculate the time averaged fluxes  $F_{i\pm 1/2}$ . In  
127 Kurganov et al. (2002) the time averaged inter-cell flux is approximated by

$$128 \quad F_{i+1/2} = \frac{a_{i+1/2}^+ f(q_{i+1/2}^-) - a_{i+1/2}^- f(q_{i+1/2}^+)}{a_{i+1/2}^+ - a_{i+1/2}^-} + \frac{a_{i+1/2}^+ a_{i+1/2}^-}{a_{i+1/2}^+ - a_{i+1/2}^-} \left[ q_{i+1/2}^+ - q_{i+1/2}^- \right] \quad (7)$$

$$129$$

130 where  $f$  is the instantaneous flux of the conserved quantity  $q$  evaluated using the recon-  
 131 structed values from the cells that border the cell interface  $x_{i+1/2}$ . While  $a_{i+1/2}^-$  and  $a_{i+1/2}^+$   
 132 are given by

$$133 \quad 134 \quad a_{i+\frac{1}{2}}^- = \min \left[ \lambda_1 \left( q_{i+\frac{1}{2}}^- \right), \lambda_1 \left( q_{i+\frac{1}{2}}^+ \right), 0 \right]$$

135 and

$$136 \quad 137 \quad a_{i+\frac{1}{2}}^+ = \max \left[ \lambda_2 \left( q_{i+\frac{1}{2}}^- \right), \lambda_2 \left( q_{i+\frac{1}{2}}^+ \right), 0 \right]$$

138 where  $\lambda_1$  and  $\lambda_2$  are estimates of the smallest and largest eigenvalues respectively of the  
 139 Jacobian.

#### 140 Propagation Speeds of a Local Shock

141 As demonstrated in Zoppou (2014)  $\lambda_1$  and  $\lambda_2$  are bounded by the phase speed of the  
 142 shallow water wave equations, so that

$$143 \quad \lambda_1 := u - \sqrt{gh} \leq v_p \leq u + \sqrt{gh} =: \lambda_2$$

144 where  $v_p$  is the phase speed of the Serre equations, thus  $a_{i+1/2}^-$  and  $a_{i+1/2}^+$  are fully deter-  
 145 mined.

#### 146 Reconstruction

147 The quantities  $q_{i+1/2}^-$  and  $q_{i+1/2}^+$  in (7) are given by the two reconstructions at  $x_{i+1/2}$ ,  
 148 one from the cell to the left  $[x_{i-1/2}, x_{i+1/2}]$  and one from the cell to the right  $[x_{i+1/2}, x_{i+3/2}]$   
 149 denoted by the superscripts  $-$  and  $+$  respectively. The order of the polynomials used  
 150 to reconstruct the quantities inside the cells determines the spatial order of the method.  
 151 Constant polynomials result in a first-order method (Godunov 1959). Similarly first- and  
 152 second-degree polynomials result in second- and third-order methods respectively.

153 For a zero-degree polynomial the interpolant has the value  $\bar{q}_i$  at  $x_i$ , this is also the  
 154 case for linear interpolation functions. For the zero-degree case the interpolants are fully  
 155 determined i.e  $q_{i-1/2}^+ = \bar{q}_i = q_{i+1/2}^-$  and monotinicity preserving. There are a variety of  
 156 ways to construct higher-degree interpolants not all of which are necessarily monotonicity  
 157 preserving, which can result in the introduction of numerical oscillations during the re-  
 158 construction process. To suppress these non-physical oscillations in higher order methods  
 159 limiting must be implemented. For the second-order method the minmod limiter was used  
 160 as in Kurganov et al. (2002). While for the third-order method the Koren limiter was used  
 161 (Koren 1993). This results in the following reconstruction scheme for the second-order  
 162 method

$$164 \quad 165 \quad q_{i+\frac{1}{2}}^- = \bar{q}_i + a_i \frac{\Delta x}{2}$$

166 and

167

168

$$q_{i+\frac{1}{2}}^+ = \bar{q}_{i+1} - a_{i+1} \frac{\Delta x}{2}$$

169 where

170

171

$$a_i = \text{minmod} \left\{ \theta \frac{\bar{q}_{i+1} - \bar{q}_i}{\Delta x}, \frac{\bar{q}_{i+1} - \bar{q}_{i-1}}{2\Delta x}, \theta \frac{\bar{q}_i - \bar{q}_{i-1}}{\Delta x} \right\} \quad \text{for } \theta \in [1, 2].$$

172 While for the third-order method the reconstruction scheme is

173

174

$$q_{i+\frac{1}{2}}^- = \bar{q}_i + \frac{1}{2} \phi^-(r_i) (\bar{q}_i - \bar{q}_{i-1})$$

175 and

176

177

$$q_{i+\frac{1}{2}}^+ = \bar{q}_i - \frac{1}{2} \phi^+(r_i) (\bar{q}_i - \bar{q}_{i-1})$$

178 where

179

180

181

$$\phi^-(r_i) = \max \left[ 0, \min \left[ 2r_i, \frac{1+2r_i}{3}, 2 \right] \right],$$

182

183

$$\phi^+(r_i) = \max \left[ 0, \min \left[ 2r_i, \frac{2+r_i}{3}, 2 \right] \right]$$

184 and

185

186

$$r_i = \frac{\bar{q}_{i+1} - \bar{q}_i}{\bar{q}_i - \bar{q}_{i-1}}.$$

187 **Fully discrete approximations to the instantaneous flux  $f(q_{i+\frac{1}{2}}^\pm)$**

188 For water depth, the fully discrete approximation to  $f(h_{i+1/2}^\pm)$  is given by

189

190

$$f\left(h_{i+\frac{1}{2}}^\pm\right) = u_{i+\frac{1}{2}}^\pm h_{i+\frac{1}{2}}^\pm$$

191 which is independent of the order of accuracy of the method.

192 The flux  $f(G_{i+1/2}^\pm)$  is more complicated because of the derivative and is given by

193

194

$$f\left(G_{i+\frac{1}{2}}^\pm\right) = u_{i+\frac{1}{2}}^\pm G_{i+\frac{1}{2}}^\pm + \frac{g\left(h_{i+\frac{1}{2}}^\pm\right)^2}{2} - \frac{2\left(h_{i+\frac{1}{2}}^\pm\right)^3}{3} \left[ \left( \frac{\partial u}{\partial x} \right)_{i+\frac{1}{2}}^\pm \right]^2.$$

195 There are multiple ways to approximate this derivative. The first- and third-order approx-  
 196 imations to the derivatives can be obtained by an upwind finite difference approximation.  
 197 By assuming that  $u$  is continuous, a second-order approximation that has the correct order  
 198 and is simpler to implement than its corresponding upwind finite difference approximation  
 199 can be used. Thus the following approximations to the derivatives were obtained for the  
 200 first-order method

201 
$$\left( \frac{\partial u}{\partial x} \right)_{i+\frac{1}{2}}^+ = \frac{u_{i+\frac{3}{2}}^+ - u_{i+\frac{1}{2}}^+}{\Delta x},$$
  
 202  
 203

204 
$$\left( \frac{\partial u}{\partial x} \right)_{i+\frac{1}{2}}^- = \frac{u_{i+\frac{1}{2}}^- - u_{i-\frac{1}{2}}^-}{\Delta x}.$$
  
 205

206 For the second-order method

207 
$$\left( \frac{\partial u}{\partial x} \right)_{i+\frac{1}{2}}^- = \left( \frac{\partial u}{\partial x} \right)_{i+\frac{1}{2}}^+ = \frac{u_{i+1} - u_i}{\Delta x}$$
  
 208

209 and for the third-order method

210 
$$\left( \frac{\partial u}{\partial x} \right)_{i+\frac{1}{2}}^+ = \frac{-u_{i+\frac{3}{2}}^+ + 4u_{i+\frac{1}{2}}^+ - 3u_{i-\frac{1}{2}}^+}{\Delta x}$$
  
 211

212 and

213 
$$\left( \frac{\partial u}{\partial x} \right)_{i+\frac{1}{2}}^- = \frac{3u_{i+\frac{1}{2}}^- - 4u_{i-\frac{1}{2}}^- + u_{i-\frac{3}{2}}^-}{\Delta x}.$$
  
 214

## 215 **Transforming between nodal values and cell averages**

216 The operator  $\mathcal{L}$  in (4) uses cell averages while the operator  $\mathcal{A}$  in (5) uses nodal values  
 217 at the cell centres. Therefore, a transformation from the cell averages to the nodal values  
 218 is required. For the first- and second-order methods this distinction is trivial since  $\bar{q}_i = q_i$ .  
 219 However, for the third-order method this is a very important distinction and failure to  
 220 handle this correctly will result in a loss of accuracy.

221 A quadratic polynomial that gives the correct cell averages for the cell centred at  $x_i$   
 222 and its two neighbours satisfies this equation

223 
$$q_i = \frac{-\bar{q}_{i+1} + 26\bar{q}_i - \bar{q}_{i-1}}{24}$$
  
 224

225 at the cell centre  $x_i$ . This is a tri-diagonal matrix equation that transforms from cell aver-  
 226 ages to nodal values with third-order accuracy and is denoted by  $\mathcal{M}$ . The inverse trans-  
 227 formation  $\mathcal{M}^{-1}$  denotes the solution of the tri-diagonal matrix equation given nodal values  
 228 resulting in cell averages which is also third-order accurate. This completes the solution  
 229 of the Serre equations (2) and (3) with the following process denoted by  $\mathcal{H}$

230

$$\mathcal{H}(\bar{\mathbf{U}}^n, \Delta t) = \begin{cases} \mathbf{U}^n &= \mathcal{M}(\bar{\mathbf{U}}^n) \\ \mathbf{u}^n &= \mathcal{A}(\mathbf{U}^n) \\ \bar{\mathbf{u}}^n &= \mathcal{M}^{-1}(\mathbf{u}^n) \\ \bar{\mathbf{U}}^{n+1} &= \mathcal{L}(\bar{\mathbf{U}}^n, \bar{\mathbf{u}}^n, \Delta t) \end{cases}.$$

231

232 **Strong-Stability-Preserving Runge-Kutta Scheme**

233 The process above is first-order accurate in time. There are many methods to increase  
 234 the accuracy of a time step evolution. This paper will use the strong stability Runge-Kutta  
 235 steps described in Gottlieb et al. (2009) to construct fully second- and third-order methods  
 236 by linear combinations of  $\mathcal{H}$ . This leads to the following processes for the first-order  
 237 method

238

$$\bar{\mathbf{U}}^{n+1} = \mathcal{H}(\bar{\mathbf{U}}^n, \Delta t)$$

239

240 the second-order method

241

$$\bar{\mathbf{U}}^{(1)} = \mathcal{H}(\bar{\mathbf{U}}^n, \Delta t),$$

242

$$\bar{\mathbf{U}}^{(2)} = \mathcal{H}(\bar{\mathbf{U}}^{(1)}, \Delta t),$$

243

$$\bar{\mathbf{U}}^{n+1} = \frac{1}{2}(\bar{\mathbf{U}}^{(1)} + \bar{\mathbf{U}}^{(2)})$$

244

245 and the third-order method

246

$$\bar{\mathbf{U}}^{(1)} = \mathcal{H}(\bar{\mathbf{U}}^n, \Delta t),$$

247

$$\bar{\mathbf{U}}^{(2)} = \mathcal{H}(\bar{\mathbf{U}}^{(1)}, \Delta t),$$

248

$$\bar{\mathbf{U}}^{(3)} = \frac{3}{4}\bar{\mathbf{U}}^n + \frac{1}{4}\bar{\mathbf{U}}^{(2)},$$

249

$$\bar{\mathbf{U}}^{(4)} = \mathcal{H}(\bar{\mathbf{U}}^{(3)}, \Delta t),$$

250

$$\bar{\mathbf{U}}^{n+1} = \frac{1}{3}\bar{\mathbf{U}}^n + \frac{2}{3}\bar{\mathbf{U}}^{(4)}.$$

251

252 **Stability Constraint**

253 A necessary condition for stability of all these explicit methods based on the finite  
 254 volume method is the Courant-Friedrichs-Lowy condition (Courant et al. 1928) which  
 255 states that

256 
$$\Delta t < \frac{\Delta x}{2 \max(|\lambda_i|)} \forall i \quad (8)$$
  
 257

258 where  $\lambda_i$  is the  $i$ th eigenvalue of the Jacobian of the flux vector.

259 **NUMERICAL SIMULATIONS**

260 The discussed methods will now be used to solve three different problems; (i) the  
 261 soliton which is an analytic solution of the Serre equations; (ii) one of the experiments  
 262 conducted by Hammack and Segur (1978) and (iii) a dam-break problem from El et al.  
 263 (2006) and Le Métayer et al. (2010). The first two will be used to validate the models,  
 264 with the soliton used to establish the order of convergence of the models. The second  
 265 problem is used to validate the models using experimental data which contains flows with  
 266 steep gradients. Lastly the dam-break problem will be used to compare the results of these  
 267 methods with those of El et al. (2006) and Le Métayer et al. (2010). The aim of which is to  
 268 verify the claim of the latter that a first-order method for the Serre equations is sufficiently  
 269 accurate to capture the important behaviour of the dam-break problem.

270 **Soliton**

271 Currently cnoidal waves are the only family of analytic solutions to the Serre equa-  
 272 tions (Carter and Cienfuegos 2011). Solitons are a particular instance of cnoidal waves  
 273 that travel without deformation and have been used to verify the convergence rates of the  
 274 proposed methods in this paper.

275 For the Serre equations the solitons have the following form

276 
$$h(x, t) = a_0 + a_1 \operatorname{sech}^2(\kappa(x - ct)), \quad (9a)$$

277 
$$u(x, t) = c \left(1 - \frac{a_0}{h(x, t)}\right), \quad (9b)$$

278 and  
 279 
$$\kappa = \frac{\sqrt{3a_1}}{2a_0 \sqrt{a_0 + a_1}} \quad (9c)$$

280 
$$c = \sqrt{g(a_0 + a_1)} \quad (9d)$$

279 where  $a_0$  and  $a_1$  are input parameters that determine the depth of the quiescent water and  
 280 the maximum height of the soliton above that respectively. In the simulation  $a_0 = 10\text{m}$ ,  
 281  $a_1 = 1\text{m}$  for  $x \in [-500\text{m}, 1500\text{m}]$  and  $t \in [0\text{s}, 100\text{s}]$ . With  $\Delta t = 0.01\Delta x$  which satisfies (8)  
 282 and  $\theta = 1.2$  for the second-order reconstruction. The example results for  $\Delta x = 100/2^6\text{m}$   
 283 can be seen in Figure 2.

284 Figure 2 demonstrates the superiority of the second- and third-order methods compared  
 285 to the first-order method. With the first-order method there is significant attenuation of the  
 286 wave due to its diffusive behaviour which creates a wider wave profile and some smaller  
 287 trailing waves. However, the first-order method does produce the correct speed of the  
 288 wave with a small phase error. While the second- and third-order methods demonstrate no  
 289 noticeable deformation resolving the soliton solution well on a relatively coarse grid with  
 290 less than 500 cells defining the actual wave.

291 The relative error as measured by the  $L_1$ -norm of the method can be seen in Figure 3.  
 292 For a vector  $\mathbf{q}$  and an approximation to it  $\mathbf{q}^*$  the relative error as measured by the  $L_1$ -norm  
 293 is

$$294 \quad L_1(\mathbf{q}, \mathbf{q}^*) = \frac{\sum_{i=1}^m |q_i - q_i^*|}{\sum_{i=1}^m |q_i|}.$$

$$295$$

296 Figure 3 demonstrates that the methods all have the correct order of convergence in  
 297 both time and space. However, this order of convergence is not uniform over all  $\Delta x$ . When  
 298  $\Delta x$  is large the actual problem is not discretised well since the cells are too large to ade-  
 299 quately resolve the problem; this causes the observed suboptimal rate of convergence in  
 300 Figure 3. When  $\Delta x$  is sufficiently small the numerical errors become small enough that  
 301 floating point errors are significant and this can also lead to suboptimal rates of conver-  
 302 gence as can be seen for the third-order method in Figure 3(c). Therefore, the order of  
 303 convergence for all methods is confirmed.

304 Figure 3 also demonstrates the superiority of the second- and third-order methods over  
 305 the first-order method for accuracy. The third-order method is also better than the second-  
 306 order method in this respect although this difference is less pronounced. These differences  
 307 have a significant impact on run-time if one wishes to run a simulation up to a desired  
 308 accuracy. A comparison of the methods for such a problem is presented in Table 1.

309 The first-order method has a runtime two orders of magnitude greater than the second-  
 310 and third-order methods. Which is sensible because the difference in  $\Delta x$  is also two orders  
 311 of magnitude. This is computationally restrictive as running practical problems to a rea-  
 312 sonable accuracy can have run times in the order of days. In particular this demonstrates  
 313 that although the second- and third- order methods are more computationally complex than  
 314 the first-order method this complexity is justified if one wants to numerically solve the  
 315 Serre equations up to some desired accuracy. This also demonstrates that a second-order

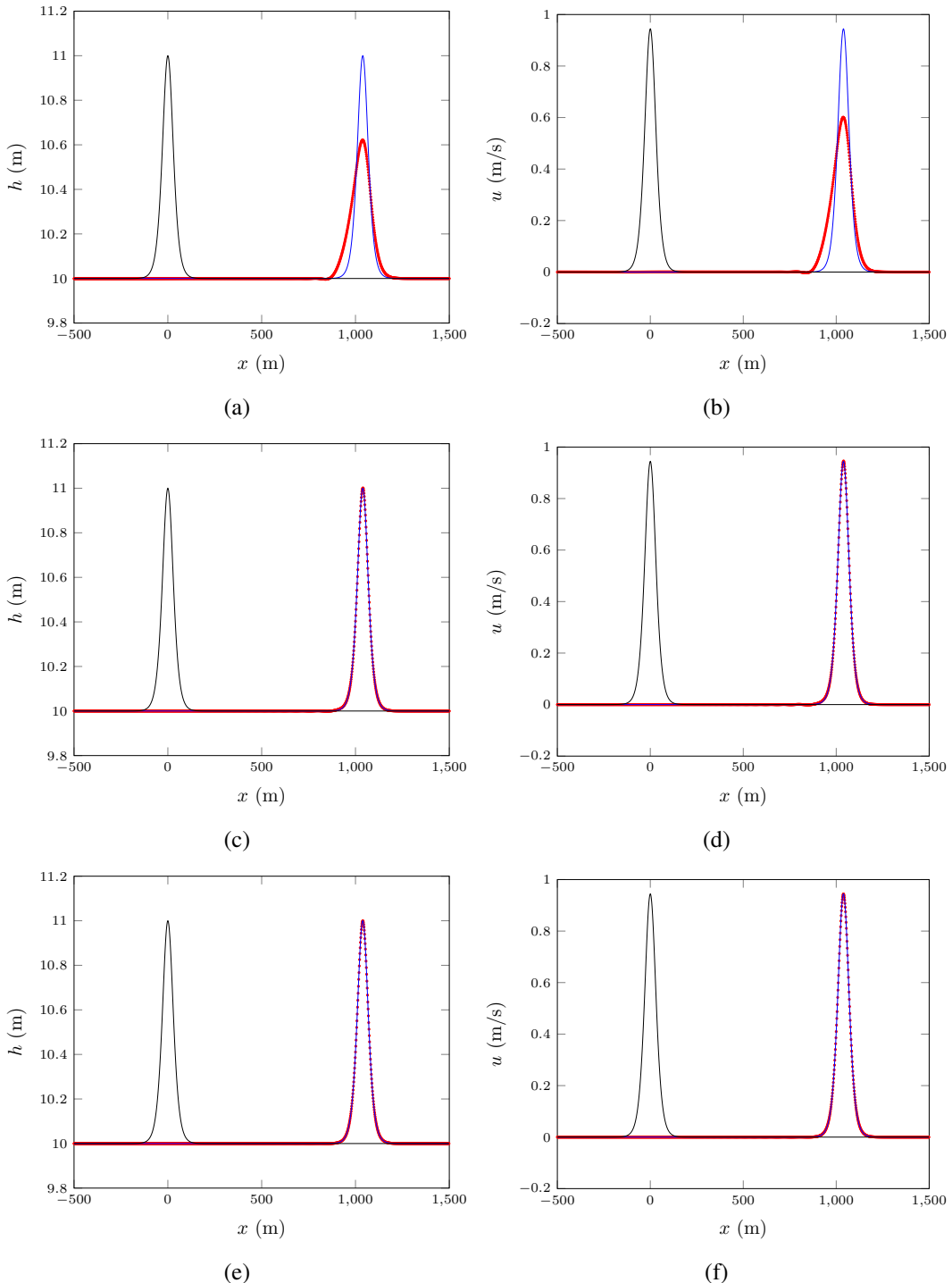


FIG. 2: The first-, second- and third-order simulation of a soliton with  $\Delta x = 100/2^6$ m ( $\circ$ ) plotted against the analytic solution of (9) (—) with black for  $t = 0$ s and blue for  $t = 100$ s.

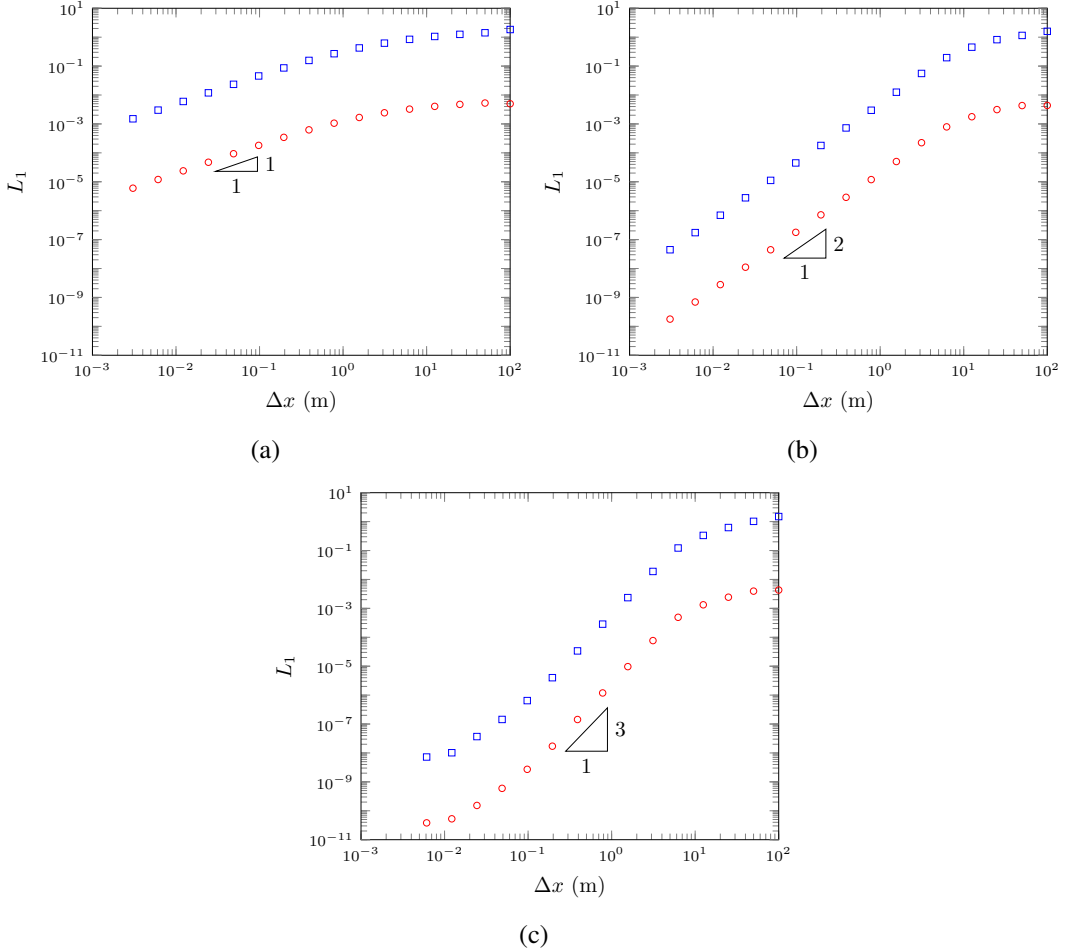


FIG. 3: Convergence of relative error using  $L_1$  norm for analytic soliton solution for both  $h$  ( $\circ$ ) and  $u$  ( $\diamond$ ) for the; (a) first-, (b) second- and (c) third-order methods.

method is adequate compared to the third-order method for solving the Serre equations up to some desired accuracy.

Figure 3(b) and Figure 3(c) demonstrate that the second- and third-order methods both have similar errors and Figure 2 shows that these methods resolve the problem well. Therefore, the extra effort in running a third-order method compared to a second-order method is not justified in this case. While the effort required to go from a first-order to a second-order method is justified since attaining a similar accuracy between them requires a restrictively small  $\Delta x$  for a first-order method.

Order	$\Delta x$ (m)	$L_1$ relative error for $h$	$L_1$ relative error for $u$	Run Time (s)
First	$100/2^{11}$	$9.32715378271 \times 10^{-5}$	$2.34320597345 \times 10^{-2}$	481.216886997
Second	$100/2^6$	$5.00595847273 \times 10^{-5}$	$1.25175521776 \times 10^{-2}$	2.19665694237
Third	$100/2^5$	$7.681432554 \times 10^{-5}$	$1.89115440455 \times 10^{-2}$	1.3766579628

TABLE 1: Comparison of run times for different order methods to get similar relative error as measured by the  $L_1$  norm for  $h$

### 324 Segur Laboratory Experiment

325 Hammack and Segur (1978) conducted an experiment that produced rectangular waves  
 326 with the stroke of a 0.61m long piston flush with the wall of a wave tank 31.6m in length.  
 327 The water height was recorded at 0m, 5m, 10m, 15m and 20m from the edge of the piston  
 328 furthest from the wall over time. The quiescent water height  $h_1$  was 0.1m while the stroke  
 329 of the piston caused a depression of water which was  $h_0 = 0.095$ m deep. To run this as  
 330 a numerical simulation the reflected problem was used. Thus the initial conditions were  
 331 reflected around the origin and  $h_1 - h_0$  was doubled by setting  $h_0 = 0.09$ m. The domain  
 332 was chosen to be from -60m to 60m and the simulation was run for 50s with  $\Delta x = 0.01$ m,  
 333  $\lambda = 0.2/\sqrt{gh_1}$ m/s and  $\theta = 1.2$ . The results of this simulation are displayed in Figures 4 -  
 334 6.

335 In this experiment for the positive side of the axis the initial depression causes a right  
 336 going rarefaction fan and a left going shock. The shocks from both sides then reflect at  
 337 the origin and so the shock and the rarefaction fan will travel in the same direction. The  
 338 leading wave in all the related figures is the rarefaction fan while the trailing dispersive  
 339 waves are the result of the reflected shock.

340 From all the related figures it can be seen that all models show good agreement be-  
 341 tween the arrival of the first wave and the period of all the waves. While Figure 4 shows  
 342 the first-order model is too diffusive and thus under estimates the heights of the dispersive  
 343 waves. Whereas the second- and third-order methods over estimate them. This overes-  
 344 timation can be explained by the Serre equations not taking into account viscous effects  
 345 that may diffuse the dispersive waves and so the results could be considered as an upper  
 346 bound on the wave heights for fluids with viscosity. Although even without these effects  
 347 these numerical methods show good agreement with the experimental data thus validat-  
 348 ing them to provide a reasonable representation of rapidly-varying flows. Additionally,  
 349 it demonstrates that the oscillations observed by the produced numerical solutions of the  
 350 Serre equations around steep gradients are physical and not numerical. In these simula-  
 351 tions the numerical oscillations that the second-order method should produce (Zoppou and  
 352 Roberts 1996) do not have a significant influence on the physical oscillations.

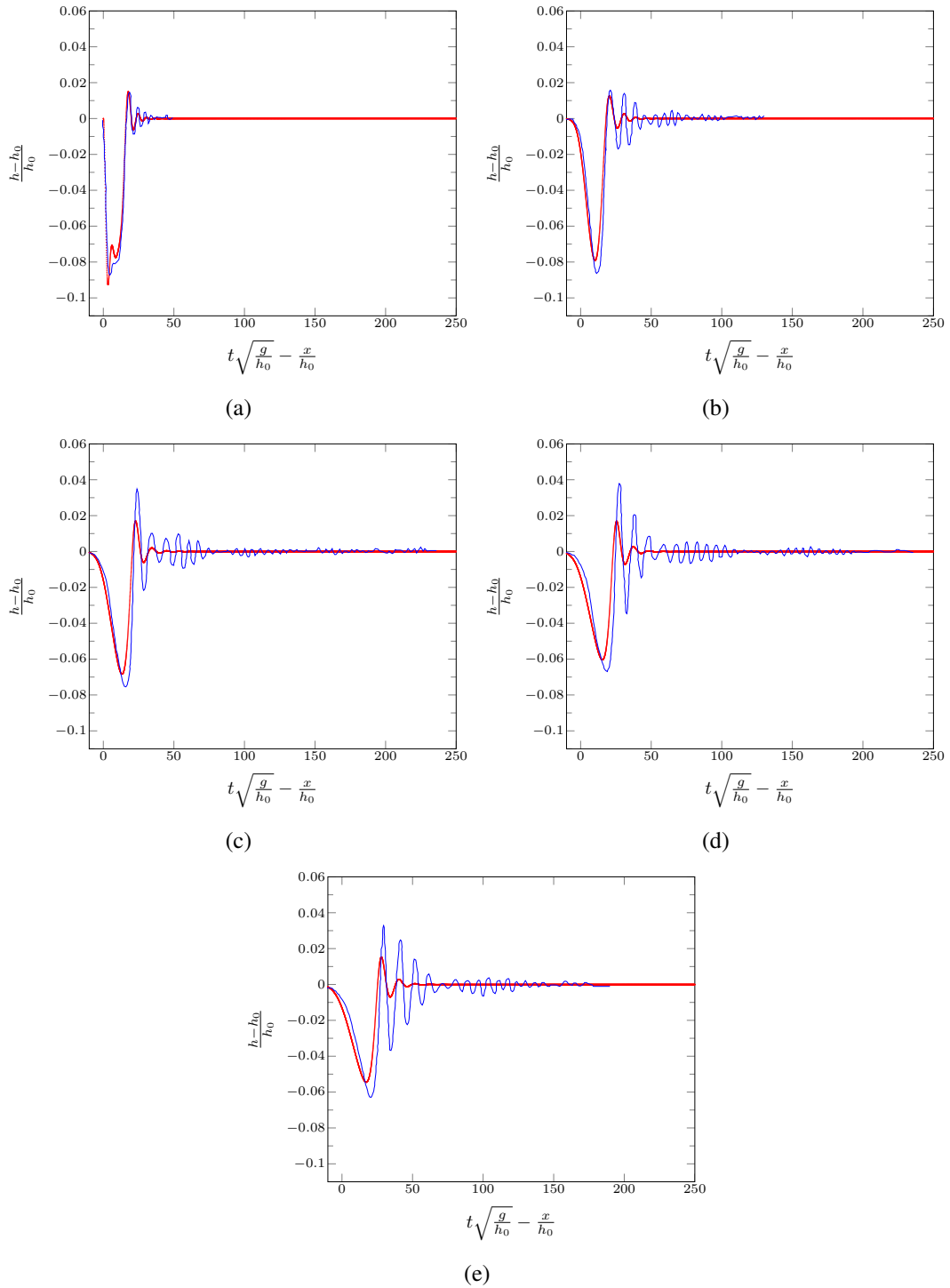


FIG. 4: Simulation of the rectangular wave experiment using the for first-order method at  $x/h_0$  : (a) 0, (b) 50, (c) 100, (d) 150 and (e) 200.

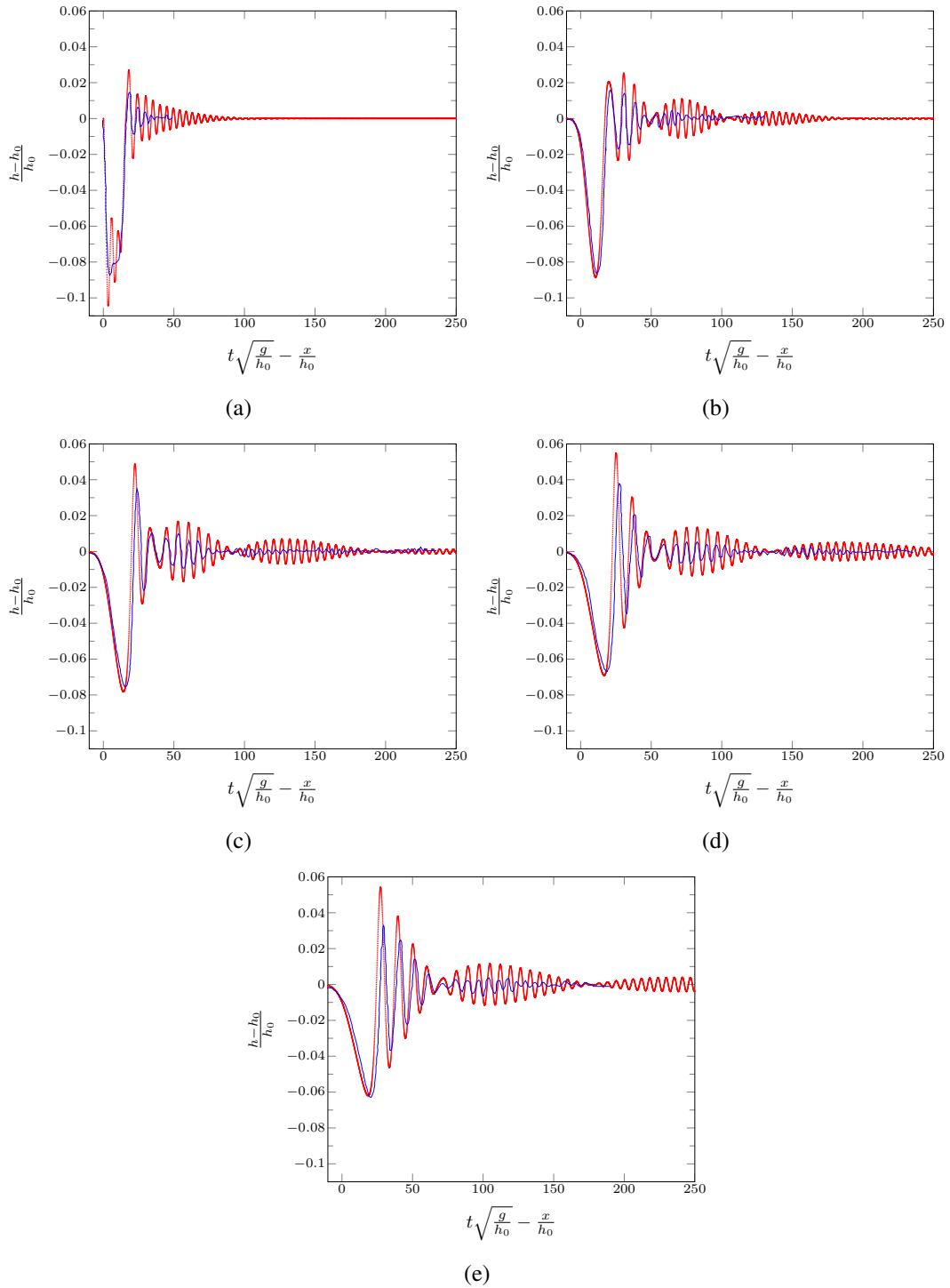


FIG. 5: Simulation of the rectangular wave experiment using the for second-order method at  $x/h_0$  : (a) 0, (b) 50, (c) 100, (d) 150 and (e) 200.

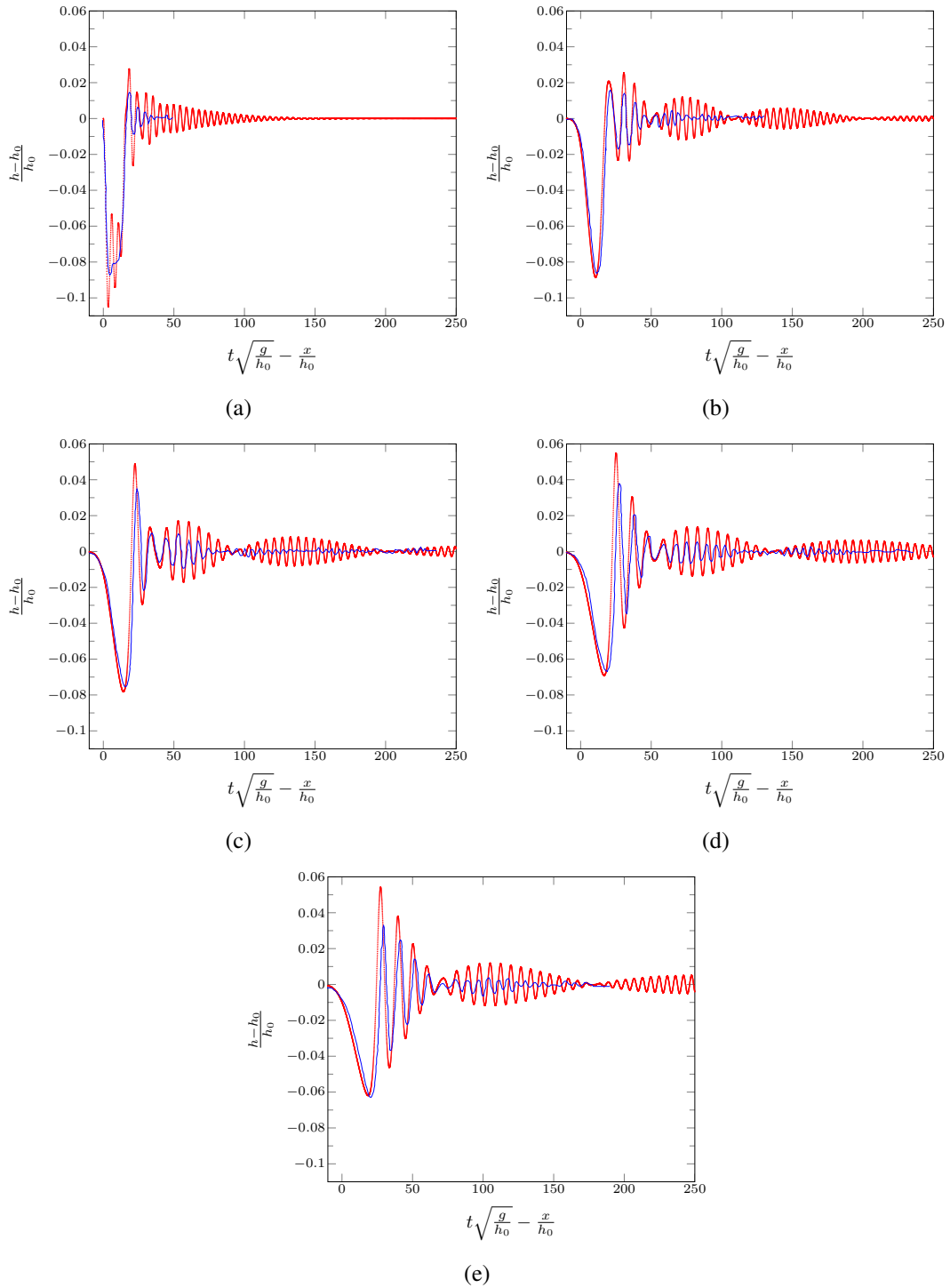


FIG. 6: Simulation of the rectangular wave experiment using the for third-order method at  $x/h_0$  : (a) 0, (b) 50, (c) 100, (d) 150 and (e) 200.

353 **Dam-Break**

354 The dam-break problem of interest can be defined as such

$$355 \quad h(x, 0) = \begin{cases} 1.8 & x < 500 \\ 1.0 & x \geq 500 \end{cases},$$

$$356 \quad u(x, 0) = 0.0m/s.$$

357 With  $x \in [0m, 1000m]$  for  $t \in [0s, 30s]$ . Where  $\lambda = 0.01m/s$  and  $\theta = 1.2$ . This corresponds  
 358 to sub-critical flow and was a situation demonstrated in El et al. (2006) and Le Métayer  
 359 et al. (2010). An example was plotted for  $\Delta x = 100/2^{10}m$  for all the methods and for  
 360  $\Delta x = 100/2^{15}m$  for the first-order method in Figure 8(d). To determine if the oscillations  
 361 that occur in the solution indeed converge to some limit as  $\Delta x \rightarrow 0$  multiple  $\Delta x$  values  
 362 were run and then the amount of variation in the solution measured. This measured how  
 363 oscillatory the solution was and was used to determine the growth of the oscillations. A  
 364 common way to measure this is the total variation  $TV$  (LeVeque 2002) which for  $\mathbf{q}$  is given  
 365 by

$$366 \quad TV(\mathbf{q}) = \sum_{\forall i>1} |q_i - q_{i-1}|.$$

$$367$$

368 If the solution does indeed converge then the  $TV$  must at some point plateau, bounding  
 369 the oscillations. This was indeed the findings of the experiments as can be seen by Fig-  
 370 ure 7. The  $TV$  increases as  $\Delta x$  decreased because the models resolved more dispersive  
 371 waves. As  $\Delta x$  decreased further the  $TV$  plateaued and so the size and number of oscilla-  
 372 tions was bounded. Therefore, the method has not become unstable which supports the  
 373 argument that the numerical methods do not introduce non-physical oscillations in the so-  
 374 lution. Under this measure the second-order method converges rapidly to the solution of  
 375 the third-order method.

376 These solutions compare very well to the findings in El et al. (2006) with both the  
 377 second- and third-order methods resolving the oscillations around the “contact discontinu-  
 378 ity”(El et al. 2006) between the rarefaction fan and the shock. In Le Métayer et al. (2010)  
 379 it was reported that for their first-order method such oscillatory behaviour was not seen.  
 380 However, for the first-order method proposed in this paper when  $\Delta x = 100/2^{15}$  it was  
 381 resolved as in Figure 8(d). This validates the findings in El et al. (2006). Interestingly this  
 382 is a much higher resolution than one needs to represent the waves themselves. It appears  
 383 that the behaviour of the dispersive waves around a steep gradient is sensitive to diffusion  
 384 so that even though the first-order method in Figure 8(a) heuristically had enough cells to  
 385 resolve most of the wave train, due to strong diffusion hardly any of the wave train was  
 386 resolved.

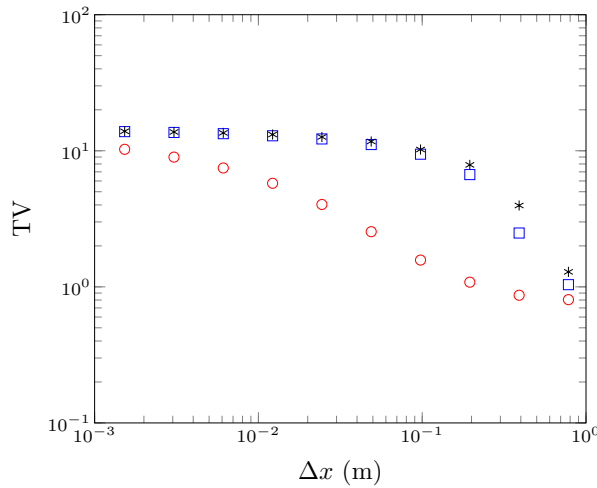


FIG. 7: The change in total variation (TV) over  $\Delta x$  for; (○) first-, (□) second-, and (\*) third-order methods.

387 There is a good agreement between the second- and third-order simulations of the dam-  
 388 break problem as can be seen in Figures 8(b) and 8(c). Although more oscillations are  
 389 resolved by the third-order method over the second-order method, there is no significant  
 390 change in the resolved behaviour of this problem between the two methods. As noted in  
 391 the introduction second-order errors are dissipative; since the diffusive third-order method  
 392 resolved the same oscillations it was demonstrated that none of the dissipative errors sig-  
 393 nificantly polluted the wave train and so the second-order method is capable of resolving  
 394 the problem well.

### 395 CONCLUSIONS

396 First-, second- and third-order hybrid finite difference-volume methods were devel-  
 397 oped to solve the Serre equations written in conservative law form. The methods were then  
 398 tested and validated. Firstly the order of the methods were all verified, secondly the meth-  
 399 ods steep gradient handling capability was validated by comparison with experimental  
 400 data. Thirdly the behaviour of the solutions matched previous findings in El et al. (2006).  
 401 Thus it can be concluded that these methods are all valid and they properly handle steep  
 402 gradients. It was also demonstrated that for these equations although second-order is not  
 403 as accurate as third-order it still provides a satisfactory method for reasonable  $\Delta x$  unlike  
 404 the first-order method which due to strong diffusion requires computationally restrictive  
 405  $\Delta x$  to produce satisfactory accuracy. So practical problems require at least a second-order  
 406 method to solve the Serre equations.

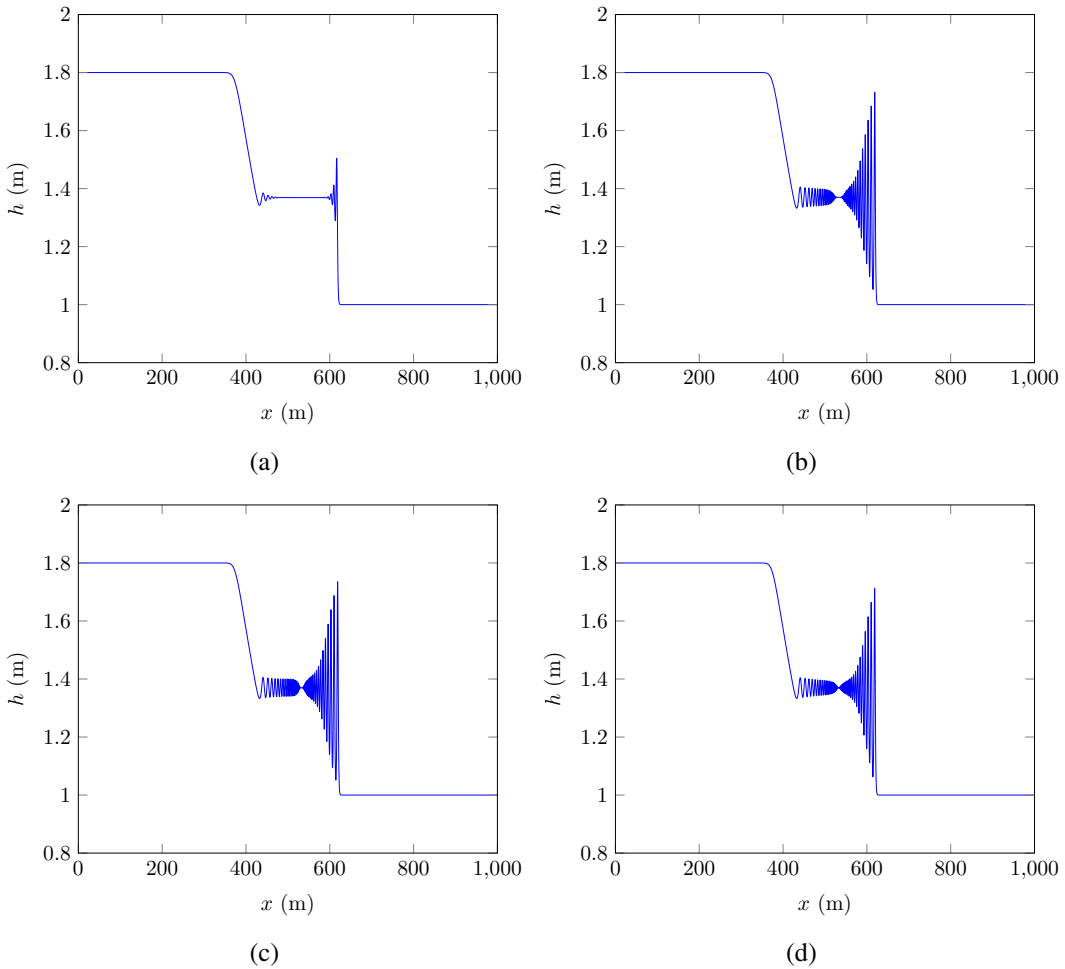


FIG. 8: Solution of the dam-break problem using the (a) first-, (b) second- and (c) third-order method with  $\Delta x = 100/2^{10}\text{m}$ . As well as a (d) first-order method with  $\Delta x = 100/2^{15}\text{m}$ .

407 **ACKNOWLEDGEMENTS**

408 Dr David George, Cascades Volcano Observatory, U.S. Geological Survey for providing  
409 the rectangular wave data.

410 **REFERENCES**

- 411 Antunes do Carmo, A., Seabra-Santos, F. J., and Almeida, A. B. (1993). “Numerical solu-  
412 tion of the generalized Serre equations with the MacCormack finite-difference scheme.”  
413 *International Journal for Numerical Methods in Fluids*, 16(8), 725–738.

- 414 Bonneton, P., Chazel, F., Lannes, D., Marche, F., and Tissier, M. (2011). “A splitting  
 415 approach for the fully nonlinear and weakly dispersive Green-Naghdi model.” *Journal*  
 416 *of Computational Physics*, 230(4), 1479–1498.
- 417 Carter, J. D. and Cienfuegos, R. (2011). “Solitary and cnoidal wave solutions of the Serre  
 418 equations and their stability.” *European Journal of Mechanics B/Fluids*, 30(3), 259–268.
- 419 Chazel, F., Lannes, D., and Marche, F. (2011). “Numerical simulation of strongly nonlin-  
 420 ear and dispersive waves using a Green-Naghdi model.” *Journal of Scientific Comput-  
 421 ing*, 48(1-3), 105–116.
- 422 Cienfuegos, R. and Barthélemy, E. and Bonneton, P. (2006). “A fourth-order compact finite  
 423 volume scheme for fully nonlinear and weakly dispersive Boussinesq-type equations.  
 424 Part i: model development and analysis.” *International Journal for Numerical Methods*  
 425 *in Fluids*, 51, 1217–1253.
- 426 Cienfuegos, R. and Barthélemy, E. and Bonneton, P. (2007). “A fourth-order compact fi-  
 427 nite volume scheme for fully nonlinear and weakly dispersive Boussinesq-type equa-  
 428 tions. Part ii: Boundary conditions and validation.” *International Journal for Numerical*  
 429 *Methods in Fluids*, 53, 1423–1455.
- 430 Courant, R., Friedrichs, K., and Lewy, H. (1928). “Über die partiellen Differenzengle-  
 431 ichungen der mathematischen physik.” *Mathematische Annalen*, 100(1), 32 – 74.
- 432 Dutykh, D., Clamond, D., Milewski, P., and Mitsotakis, D. (2011). “Finite volume and  
 433 pseudo-spectral schemes for the fully nonlinear ‘irrotational’ Serre equations.” *Arxiv*,  
 434 24(5), 0 – 25.
- 435 El, G., Grimshaw, R. H. J., and Smyth, N. F. (2006). “Unsteady undular bores in fully  
 436 nonlinear shallow-water theory.” *Physics of Fluids*, 18(027104).
- 437 Godunov, S. K. (1959). “A difference method for numerical calculation of discontinuous  
 438 solutions of the equations of hydrodynamics.” *Matematicheskii Sbornik*, 89(3), 271–  
 439 306.
- 440 Gottlieb, S., Ketcheson, D. I., and Shu, C. W. (2009). “High order strong stability preserv-  
 441 ing time discretizations.” *Journal of Scientific Computing*, 38(3), 251–289.
- 442 Green, A. E. and Naghdi, P. M. (1976). “A derivation of equations for wave propagation  
 443 in water of variable depth.” *Journal of Fluid Mechanics*, 78(2), 237–246.
- 444 Hammack, J. L. and Segur, H. (1978). “The Korteweg-de Vries equation and water waves.  
 445 Part 3. Oscillatory waves.” *Journal of Fluid Mechanics*, 84(2), 337–358.
- 446 Koren, B. (1993). “A robust upwind discretization method for advection, diffusion and  
 447 source terms.” *Notes on Numerical Fluid Mechanics*, Vol. 45, Centrum voor Wiskunde  
 448 en Informatica, Amsterdam.
- 449 Kurganov, A., Noelle, S., and Petrova, G. (2002). “Semidiscrete central-upwind schemes  
 450 for hyperbolic conservation laws and Hamilton-Jacobi equations.” *Journal of Scientific*  
 451 *Computing, Society for Industrial and Applied Mathematics*, 23(3), 707–740.

- 452 Lannes, D. and Bonneton, P. (2009). "Physics of Fluids, 21(1), 16601–16610.
- 453 Le Métayer, O., Gavrilyuk, S., and Hank, S. (2010). "A numerical scheme for the Green-  
454 Naghdi model." *Journal of Computational Physics*, 229(6), 2034–2045.
- 455 LeVeque, R. (2002). *Finite Volume Methods for Hyperbolic Problems*, Vol. 54 of *Cam-  
456 bridge Texts in Applied Mathematics*. Cambridge University Press.
- 457 Li, M., Guyenne, P., Li, F., and Xu, L. (2014). "High order well-balanced CDG-FE meth-  
458 ods for shallow water waves by a Green-Naghdi model." *Journal of Computational  
459 Physics*, 257, 169–192.
- 460 Mitsotakis, D., Ilan, B., and Dutykh, D. (2014). "On the Galerkin/Finite-Element Method  
461 for the Serre Equations." *Journal of Scientific Computing*, 61(1), 166–195.
- 462 Serre, F. (1953). "Contribution à l'étude des écoulements permanents et variables dans les  
463 canaux." *La Houille Blanche*, 6, 830–872.
- 464 Su, C. H. and Gardner, C. S. (1969). "Korteweg-de Vries equation and generalisations.  
465 III. Derivation of the Korteweg-de Vries equation and Burgers equation." *Journal of  
466 Mathematical Physics*, 10(3), 536–539.
- 467 Zoppou, C. (2014). "Numerical solution of the One-dimensional and Cylindrical Serre  
468 Equations for Rapidly Varying Free Surface Flows." Ph.D. thesis, Australian National  
469 University, Australian National University.
- 470 Zoppou, C. and Roberts, S. (1996). "Behaviour of finite difference schemes for advection  
471 diffusion equations." *Technical Report Mathematics Research Report No.MRR 062-96*.